Geochemistry Geophysics Geosystems G3

Article
Volume 00, Number 00
0 MONTH 2013
doi: 10.1002/ggge.20211
ISSN: 1525-2027

Published by AGU and the Geochemical Society

Crustal structure along the Aleutian island arc: New insights from receiver functions constrained by active-source data

Helen A. Janiszewski, Geoffrey A. Abers, and Donna J. Shillington
Columbia University, Lamont Doherty Earth Observatory, Palisades, New York, 10964, USA (helenj@ldeo.columbia.edu)

Josh A. Calkins
Transform Software and Services, Littleton, Colorado, USA

[1] Moho depth and Vp/Vs estimates from stacking phases of receiver functions along the Aleutian island arc give new constraints on its composition and structure. They expand on the current understanding of island arcs and their relationship to continental crust production. We also present an approach for including constraints from active-source data in receiver function analysis in a region with sparse data coverage to complement this analysis. Moho depth averages 37.5 km with an average uncertainty of 2.5 km along the entire arc. Excluding the westernmost island of Attu yields an average crustal thickness of 38.5 ± 2.9 km. The Vp/Vs ratio decreases moving eastward along the arc with an average value of 1.80 in the western and central portion of the arc built on oceanic crust, but 1.63 in the eastern section built on continental crust. This may reflect tectonic and compositional changes along the arc. However, overall the arc appears more mafic than continental crust. Near-constant crustal thickness, despite significant compositional changes, may indicate that nonmagmatic processes such as erosion and isostasy act to regulate arc thickness. Additionally, strong conversions from an upper crustal magma chamber are observed beneath Akutan Island, confirming and clarifying the geometry of the magma body inferred from other techniques. They indicate a volcanic body much larger than the eruptive edifice, a feature that must persist between eruptive cycles.

Components: 9,434 words, 9 figures, 2 tables.

Keywords: subduction zone; crustal thickness; Vp/Vs; continental crust; magma chamber.

Index Terms: 7240 Subduction zones: Seismology; 1207 Transient deformation: Geodesy and Gravity; 1219 Gravity anomalies and Earth structure: Geodesy and Gravity; 1240 Satellite geodesy: results: Geodesy and Gravity; 8185 Volcanic arcs: Tectonophysics; 1020 Composition of the continental crust: Geochemistry.

Received 21 March 2013; **Revised** 21 June 2013; **Accepted** 22 June 2013; **Published** 00 Month 2013.

Janiszewski, H. A., G. A. Abers, D. J. Shillington, and J. A. Calkins (2013), Crustal structure along the Aleutian island arc: New insights from receiver functions constrained by active-source data, *Geochem. Geophys. Geosyst.*, *14*, doi:10.1002/ggge.20211.

© 2013. American Geophysical Union. All Rights Reserved.

1. Introduction

[2] Although island arcs are proposed as sites of continental crust production, the process by which this crust is formed is not fully understood [*Taylor*, 1967]. Average continental crust has a bulk andesitic composition [*Christensen and Mooney*, 1995; *Rudnick and Fountain*, 1995], but existing constraints suggest that many island arcs are more basaltic [*Kay and Kay*, 1994]. Magmatic mixing and lower crustal foundering are processes that could alter island arc crust postformation, leaving behind crust similar to that of continents [*Kay and Kay*, 1988; *Rudnick*, 1995]. Under certain pressure and temperature conditions, mafic to ultramafic compositions commonly found in the lower crust may be denser than the underlying mantle, potentially allowing foundering [*Jull and Kelemen*, 2001].

[3] To examine these ideas, seismology can provide indirect estimates of the composition of island arc crust. The Aleutian island arc has been the subject of previous studies of its primary magma compositions [*Kay and Kay*, 1994; *Kelemen et al.*, 2003] and active-source seismic studies of its *P* wave velocities [*Fliedner and Klemperer*, 1999, 2000; *Holbrook et al.*, 1999; *Lizarralde et al.*, 2002; *Shillington et al.*, 2004; *Van Avendonk et al.*, 2004]. Seismic velocities have the advantage of providing estimates of composition of an intact arc by remotely imaging the crust; however, the relationship between *P* wave velocity and composition is ambiguous, particularly for mafic-ultramafic compositions [*Behn and Kelemen*, 2003]. Addition of *S* wave information can provide clearer constraints [*Behn and Kelemen*, 2006]. The Aleutian arc has an ideal history for understanding the role of island arcs in building continental crust: it is relatively free of preexisting material, and has been stable with little recent variation in volcanism or arc rifting [*Fournelle et al.*, 1994; *Kay and Kay*, 1994]. This arc is also of particular relevance to study continental crust production because the arc transitions from a continental arc to an oceanic arc near 165°W, and there are also along-strike variations in lava composition, the age of the subducting plate, convergence direction, and other subduction parameters [*Fournelle et al.*, 1994].

[4] In this study, we examine the whole arc by analyzing teleseismic waveforms recorded by permanent stations in the Aleutians. Receiver functions systematically measure crustal thickness and the ratio of *P* to *S* wave velocities (Vp/Vs), which provide improved constraints on bulk arc composition. Although sparse, seismic stations are present along the entire Aleutian arc, enabling us to quantify large-scale changes in composition and crustal thickness. Our analysis shows a westward increase in crustal-averaged Vp/Vs ratio from the continental to oceanic parts of the arc, but intriguingly, crustal thickness remains relatively constant at 38.5 ± 2.9 km for much of the arc (excluding Attu). From these results, we infer that the composition of this island arc varies between that typical of oceanic and continental arcs. Furthermore, at several volcanoes we see hints of magma chambers, and the well-sampled magma body under Akutan Island generates strong signals. The magma body appears much larger than expected, complementing previous studies of inflation and seismicity in the area [e.g., *Lu et al.*, 2000; *Ji and Herring*, 2011].

2. Methods

2.1. Data Collection and Processing

[5] We examine data from 13 permanent broadband seismometers along the Aleutian island arc recording earthquakes occurring between January 2000 and December 2008. Each station operated for at least one continuous year during this time (Figure 1 and Table 1). Earthquakes are selected from those that originated 25°–90° from a point central to the stations (54.1°N, 165.8°W), and with magnitudes between 5.0 and 7.0. Over this period, approximately 700 earthquakes meet these conditions to at least one operating station, although we used only a subset. Radial-component receiver functions are calculated in the frequency domain from the *P* wave coda [*Ammon*, 1991; *Zandt et al.*, 1995] for records that contain a visually obvious initial *P* wave arrival. Receiver functions are disregarded if the signal-to-noise ratio is <2 following deconvolution or they have obvious long-period noise. Where possible, a range of back azimuths is incorporated for each station to detect variations in structure with direction (Figure 1, inset). Because earthquakes are distributed unevenly around the planet, most signals are restricted to those with back azimuths of 70°–110° and 170°–250° relative to the stations. A total of 300 receiver functions are calculated and pass these quality criteria, with 14–46 per station.

2.2. Moveout Corrections

[6] As the *P* wave front travels through an abrupt boundary, it produces a converted Ps phase and

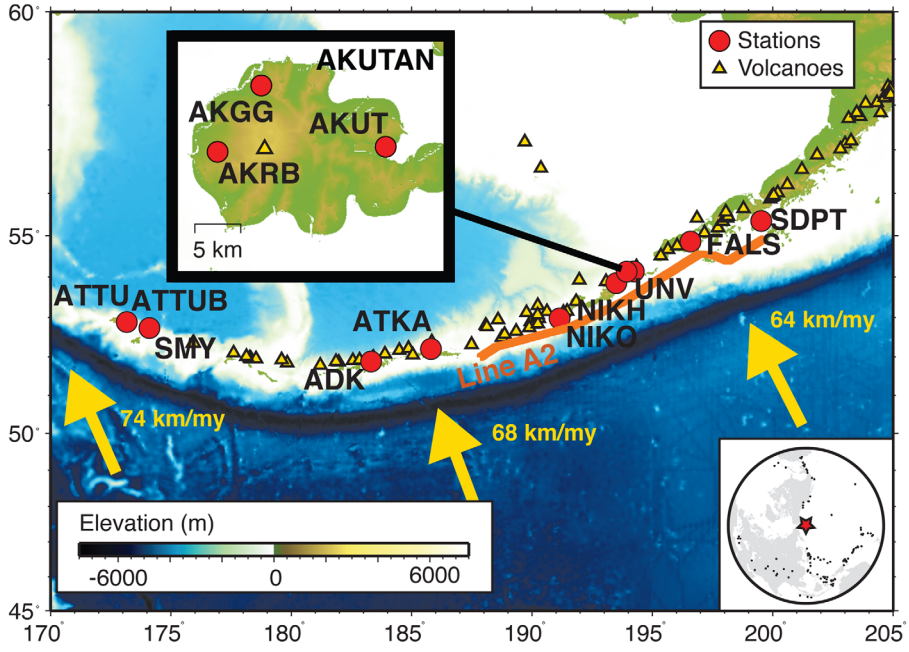

Figure 1. Locations of the seismic stations used for this study and topography of the Aleutians. Cluster of stations surrounding the volcano on Akutan Island is shown in inset. Arrows indicate the relative plate movement of the Pacific plate [*Syracuse and Abers*, 2006; *DeMets et al*., 1994]. Line A2, shown in orange, is refraction line of *Shillington et al*. [2004]. Bottom inset: Locations of earthquakes used in calculating receiver functions (black dots).

surface multiples, termed here Ppms and Psms. In this paper, we use the terminology "Ps" for the upgoing *P* to *S* conversion off the Moho, "Ppms" for the first Moho reverberation with only the last leg as S, and "Psms" as a Moho reverberation with the last two legs as S, following *Rossi et al*. [2006]. For a given Vp and Vs and ray parameter, the monotonic relationship between the depth to the Moho (or any interface) and the arrival times of each of these three phases can be inverted as a moveout correction, converting lag time to interface depth. The depths predicted for the three phases agree at the correct Vp/Vs [*Zhu and Kanamori*, 2000; *Rossi et al*., 2006]. In applying the correction, we assume a constant crustal Vp and calculate moveout-corrected traces following *Rossi et al*., [2006]. Although the Aleutians are structurally complex, a 1-D velocity assumption for each station should suffice since only a small patch under each station is sampled by the

Table 1. Stations

Station	Network[a]	Sensor	Latitude	Longitude	Receiver Functions
ATTU	IM	Geotech KS-54000 borehole	52.8821	173.1643	46
ATTUB	IM	Geotech KS-54000 borehole	52.8821	173.1643	15
SMY	AT	Streckeisen STS-2	52.7308	174.1031	24
ADK	IU	Streckeisen STS-1	51.8823	−176.6842	31
ATKA	AK	Guralp CMG3-ESP 60sec	52.2027	−174.1955	28
NIKO	AK	Guralp CMG3-ESP 60sec	52.9388	−168.8667	16
NIKH	AK	Streckeisen STS-2 G3	52.9731	−168.853	14
UNV	AK	Guralp CMG3-ESP 60sec	53.8465	−166.502	29
AKRB	AV	Guralp CMG6TD	54.1300	−166.0687	17
AKGG	AV	Guralp CMG6TD	54.1988	−165.9916	17
AKUT	AT	Streckeisen STS-2	54.1352	−165.7719	18
FALS	AK	Guralp CMG3-ESP 30sec	54.8573	−163.4155	20
SDPT	AT	Streckeisen STS-2	55.3493	−160.4766	25

[a]Network information at IRIS DMC.

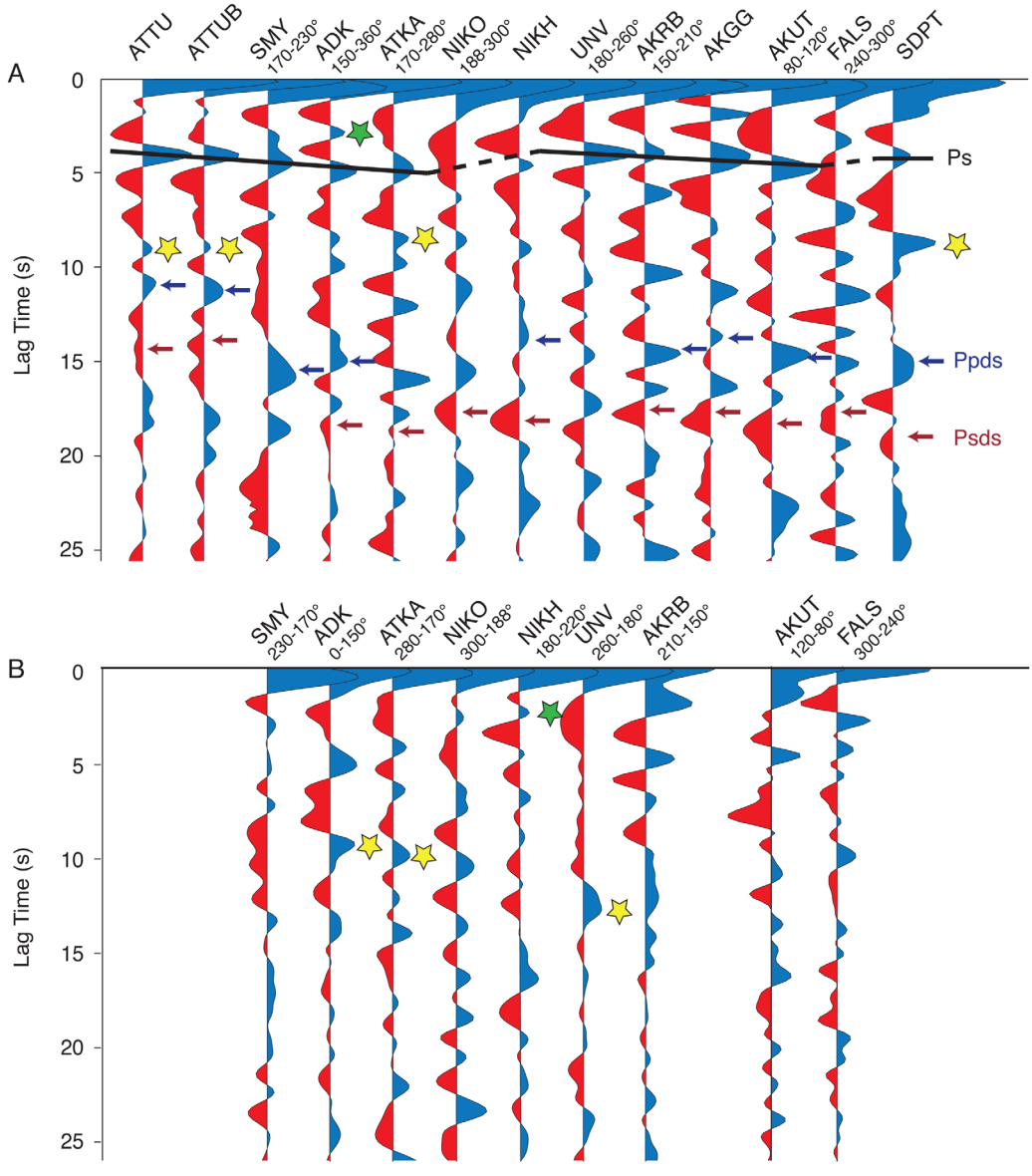

Figure 2. Stacks of receiver functions for each station. Positive arrivals are shown in blue, negative arrivals are shown in red. The lag time is measured with respect to the initial *P* wave arrival. Back-azimuth ranges included in the stack are given below the station name, for stations where multiple back-azimuth subsets were taken. (a) Includes all receiver functions used to determine the Moho depth and average crustal Vp/Vs. The Ps, Ppms, and Psms arrivals off the Moho are indicated where observed. (b) Stacks of the data that were not used for the Moho analysis, some of which show evidence for other discontinuities. Green stars indicate multiple off the midcrustal discontinuity. Yellow stars indicate the first arrival off the slab.

upcoming waves. All Ps arrivals intersect the Moho <20 km horizontal distance from the station, and most are between 5 and 15 km ([1]supporting information).

[1]Additional supporting information may be found in the online version of this article.

2.3. Inversion

[7] For each station, moveout-corrected radial-component receiver functions are stacked to reduce signal noise using the Ps, Ppms, and Psms predicted moveouts (Figure 2). A grid search similar to *Zhu and Kanamori* [2000] with error analysis from *Rossi et al.* [2006] is performed for an interface depth range of 10–60 km and Vp/Vs

Table 2. Results From Inversion for Crustal Structure

Station	Vp (km/s)[a]	Moho (km)	Moho Range (km)	Vp/Vs	Vp/Vs Range	Active-Source Moho (km)	Constrained Vp/Vs	Constrained Vp/Vs Range
ATTU	6.8	26.3[b]	25–28[b]	1.96[b]	1.88–2.05[b]			
ATTUB	6.8	27.4[b]	25–30[b]	1.94[b]	1.84–2.08[b]			
SMY[c]	6.8	40.7	39–42	1.69	1.64–1.75			
ADK[c]	6.8	36.8	35–39	1.82	1.76–1.89			
ATKA[e]	6.9	43.0[b]	41–45[b]	1.74[b]	1.68–1.80[b]	31.6[d]	1.99[d]	1.80–2.09[d]
NIKO[c]	6.8	36.4[e]	33–41[e]	1.74[e]	1.5–1.91[e]	37.4[f]	1.68[f]	1.63–1.85[f]
NIKH	6.8	35.7	34–38	1.79	1.73–1.86	35.7	1.79	1.73–1.86
UNV[c]	7.1	41.6	40–44	1.64	1.59–1.69	37.7[d]	1.70[d]	1.66–1.82[d]
AKRB[c]	6.7	39.0	37–41	1.62	1.55–1.69	37.4	1.67	1.64–1.72
AKGG	6.7	33.8	31–37	1.88	1.70–2.00	33.3	1.88	1.74–1.95
AKUT[c]	6.7	36.7	32–41	1.83	1.69–2.01	36.5	1.84	1.77–1.99
FALS[c]	6.9	41.1	39–43	1.55	1.51–1.59	39	1.59	1.56–1.64
SDPT	6.8	38.5	35–41	1.68	1.61–1.78			

[a]Vp determined from active-source data [*Shillington et al*., 2004].
[b]Only Ps and Ppms stacked.
[c]Limited back-azimuth range used in calculation.
[d]Only Ps stacked.
[e]Only Ps and Psms stacked.
[f]Only Psms stacked.

range of 1.5–2.2 above the interface, at intervals of 0.1 km and 0.01, respectively. The average crustal Vp used in the inversion is determined from the results of a wide-angle reflection/refraction study parallel to the Aleutian island arc [*Shillington et al*., 2004] (Line A2 on Figure 1). This study gives an average crustal *P* wave velocity of 6.8 km/s; stations that are not located along the active-source line use this average. Velocities for stations proximal to the refraction profile of *Shillington et al*. [2004] are vertically averaged from the refraction results near these locations. Those stations are ATKA, NIKO, NIKH, UNV, AKUT, AKRB, AKGG, and FALS, between 175°W and 162°W, for which the average crustal Vp ranged from 6.7 to 7.1 km/s (see Table 2 for details). We tested the sensitivity of our result to the assumptions about Vp by also fixing the average crustal Vp to a uniform 6.5 and 7 km/s for all stations. These values span the range observed in active-source images along strike [*Fliedner and Klemperer*, 1999; *Shillington et al*., 2004]. Within the formal errors, the depth and Vp/Vs results agreed with each other for different input Vp, indicating that this assumption does not have a significant effect on our results (Figure 6). Variations in Moho depth are roughly linear with Vp, such that this range in Vp corresponds to approximately ± 1.5 km variation. The only exception to this occurred at NIKO, where the Moho arrival is indistinct (see section 3.2.1).

[8] The inversion finds the boundary depth and crustal Vp/Vs for which the three converted phases (Ps, Ppms, and Psms) best agree (Figure 3). For each station, the three moveout-corrected and stacked signals are given weights of 1.0, 0.5, 0.1, or 0 in order of decreasing signal level according to their strength of their visual appearance in the trace. This is assessed by the relative signal-to-noise ratio of the conversions. These weights are normalized to 1.0 during the inversion. To test objectiveness of this weighting we performed the inversion using equal weights for the three multiples; the results were not statistically different.

[9] Where the character of the conversion varies with back azimuth, the receiver functions are grouped and stacked in appropriate back-azimuth ranges before being examined. If the influence from complex structure is suspected to interfere with the Moho arrivals in one or more azimuthal bins, these bins are not included in the final stacks. We also estimated crustal thickness stacking over all back azimuths, and the results were not significantly different.

[10] At some stations, two arrivals are observed in the receiver functions representing the Moho boundary and a shallower midcrustal layer (Figure 2). These features are considered reliable if they appeared in two of the three mode conversions at the same moveout-corrected depth. In this case, the inversion is performed for both boundaries separately. First, the depth and average Vp/Vs for the Moho are determined as described above. Then the process is repeated using an average Vp adjusted for a shallower layer. *Shillington et al*. [2004] also found evidence for a midcrustal interface at ~20 km. This is observed at two stations:

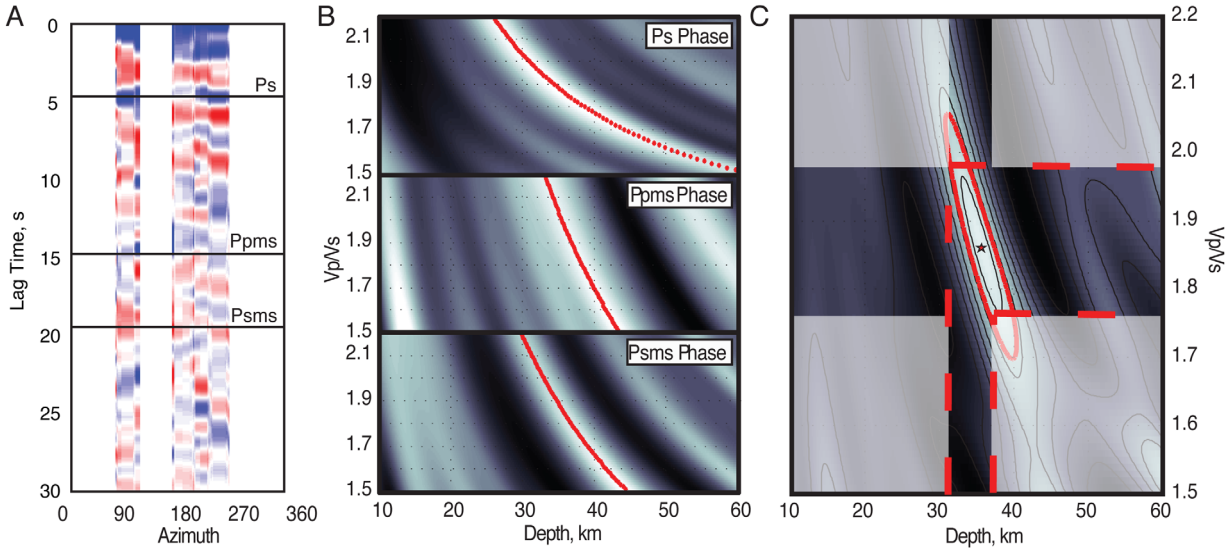

Figure 3. Example of receiver function analysis for AKUT station. (a) Receiver functions as a function of back azimuth, 0.5 Hz low-pass filter. Predicted arrival times of Moho phases are indicated. (b) Stacked amplitude as function of Moho depth and Vp/Vs, for each major phase. Estimated Moho arrival indicated by the red curves. Here each multiple is given a weight of 1. (c) Joint stack amplitude of all three phases. Star indicates the estimated Moho depth and average crustal Vp/Vs, and the red contour indicates the 85% confidence interval. For all stations coincident with *Shillington et al*. [2004] the result is improved by restricting the depth to the predicted range from the active-source study (here 35 ± 2.5 km, shown by the vertical red dotted lines). This gives a smaller range for Vp/Vs.

ADK and NIKH. At ADK we use the arc-wide average upper crustal Vp of 6.5 km/s; at NIKH upper crustal Vp = 6.3 km/s [*Shillington et al*., 2004]. Based on the tests of the sensitivity of our results to assumed Vp for the whole crust, we also assume that the results for the upper crust will not be very sensitive to Vp assumptions.

[11] For stations along the refraction profile, we also perform a set of inversions for Vp/Vs a priori restricting the depth range to the allowed boundary depths from *Shillington et al*. [2004] and *Van Avendonk et al*. [2004]. The uncertainties of the active-source Moho depth are determined from *Van Avendonk et al*. [2004]; stations in the middle of the active-source line have uncertainties of ±2.5 km, whereas those on the ends of the line (ATKA and FALS) have uncertainties of ±4 km. This procedure is particularly useful for stations and azimuth subsets that have only one clear multiple in their receiver functions, since otherwise two multiples are needed to determine the depth and Vp/Vs. Rather than correlating weak multiples, only clear conversions are used to give a potentially more robust Vp/Vs estimate. In this case, the result is dependent on both the active-source and receiver function measurements (Figure 3 and more details in supporting information). This procedure assumes that refraction and receiver functions sample the same boundary and same velocities.

[12] Following *Rossi et al*. [2006], a Student *t* test on stack amplitude is used to determine the 85% confidence ellipse for the depth and Vp/Vs result. A fixed depth corresponds to an 85% confidence interval in the two parameters, so that maximal bounds in any one parameter approximate 95% marginal confidence limits.

3. Arc-Length Crustal Structure

3.1. Results

[13] At many of the stations, the most prominent Ps conversion occurs around 5 s after the initial *P* wave arrival. The primary free-surface multiples (Ppms and Psms) are more difficult to discern, likely due to complex crustal structure (Figure 2). As a result, the full inversion frequently yields Vp/Vs estimates with large uncertainties. Results are summarized in Table 2. The sharpest boundary is located between 34 and 43 km beneath all stations excluding those on Attu. We interpret this as the Moho. The average depth at all stations is 37.5 with a 2.5 km average error and a root-mean-square (RMS) variation of ±4.3 km. Excluding

ATTU and ATTUB (which are the same station, operational at different times) yields a mean crustal thickness of 38.5 km with average error 2.6 km with a RMS variation of ±2.9 km (Figure 4). We discuss the anomalous Attu results below. The Moho typically is strong along the arc.

[14] The average Vp/Vs ratio above the Moho is 1.74 with an average error of 0.09 using the single-layer inversion [e.g., *Rossi et al*., 2006], but it ranges from 1.55 to 1.96 for individual measurements. Individual errors range up to ±0.20 although are typically <0.10. Constraining crustal thickness from the active-source data [*Shillington et al*., 2004] reduces the uncertainty in the Vp/Vs estimates. Within the eastern, continental section of the arc, this added constraint decreases the variation in Vp/Vs between stations. The average Vp/Vs is 1.77 with 0.08 average error using the active-source Moho depth constrainted results where possible (Figure 4). The variability of Vp/Vs increases for these constrained results even though on average uncertainty decreases; however, this is largely due to the result at ATKA. Excluding ATKA leads to a decrease in variation (RMS variation decrease of ∼14%). In particular, RMS variation at UNV, AKRB, AKGG, and AKUT (four stations clustered within 60 km of each other) is now ±0.10, compared to ±0.13 in the unconstrained inversion.

[15] The largest depth outliers are below the two westernmost stations, ATTU and ATTUB, where the crust is 10 km thinner than other stations. The crust appears to be anomalously thin below Attu island compared to the rest of the arc, and volcanism with magmatic addition stopped at Attu some time ago. The western Aleutians undergo more extension than the eastern and central arc, so perhaps the crust here is tectonically attenuated [*Yogodzinski et al*., 1993]. The remaining stations show relative uniformity in crustal thickness despite known changes in geologic structure from east to west.

[16] In contrast to the depth, the Vp/Vs ratios increase slightly from east to west. While a denser coverage of stations is needed to understand the nature of this variation, stations on continental crust in the Alaska Peninsula-Umnak (FALS and SDPT) have an average Vp/Vs of 1.62, while the western stations have an average of 1.77. The constrained results yield averages of 1.63 and 1.80, respectively. This change may reflect the transition of the overriding plate from continental crust east of Unimak Pass at 196° longitude to oceanic crust west of this location [*Fournelle et al*., 1994; *Fliedner and Klemperer*, 2000].

3.2. Secondary Arrivals

[17] Many stations show complicated features in their receiver functions, including variations with back azimuth and additional arrivals. Dipping layers, anisotropy, and low-velocity zones have the potential to complicate receiver functions [*Cassidy*, 1992; *Jones and Phinney*, 1998; *Nikulin et al*., 2009], as do multiple interfaces. In the Aleutians, the subducting slab and geology related to volcanism likely contribute to this complexity. The limited back-azimuthal coverage, noisy stations and the sparse geographical distribution of the stations make it difficult to find trends in this variation and thus to determine its cause, but there are some clues. A more detailed description of observations at each station is in the supporting information.

3.2.1. Midcrustal Boundary and Weakened Moho

[18] Two stations showed clear evidence of a midcrustal boundary in addition to the Moho: ADK at 24 ± 1.5 km and NIKH at 17.9 ± 2 km (Figure 2). This layering agrees with *Shillington et al*. [2004], who observed an intracrustal interface at approximately 20 km depth along their refraction line. The Vp/Vs above this boundary is similar to that for the whole crust with an average for the upper layer of 1.73; incorporating the active-source interface depths gives an average of 1.70, which is slightly lower than what we predict for the whole crust.

[19] NIKO and NIKH, located 4 km apart in Nikolski on Umnak Island in the eastern section of the island arc, appear to have a weak Moho as indicated by a lack of obvious Ps arrivals. This agrees with *Shillington et al*. [2004], who observe very high *P* wave velocities in the lower crust (∼7.6 km/s) in this part of the arc, which are only slightly lower than in the upper mantle (∼8.0–8.1 km/s). FALS also lacks a prominent Ps arrival; however, this station is at the end of the seismic line from *Shillington et al*. [2004] so it could not be compared (Figure 2).

3.2.2. Shallow Structure

[20] The initial direct *P* wave arrivals are slightly delayed in the receiver functions (<0.5 s lags) at about half the stations. Probably, shallow sedimentary basins or volcaniclastic piles generate conversions that interfere with direct *P* [*Sheehan et al*., 1995]. The data from all stations display negative polarity pulses following the initial *P* wave arrival,

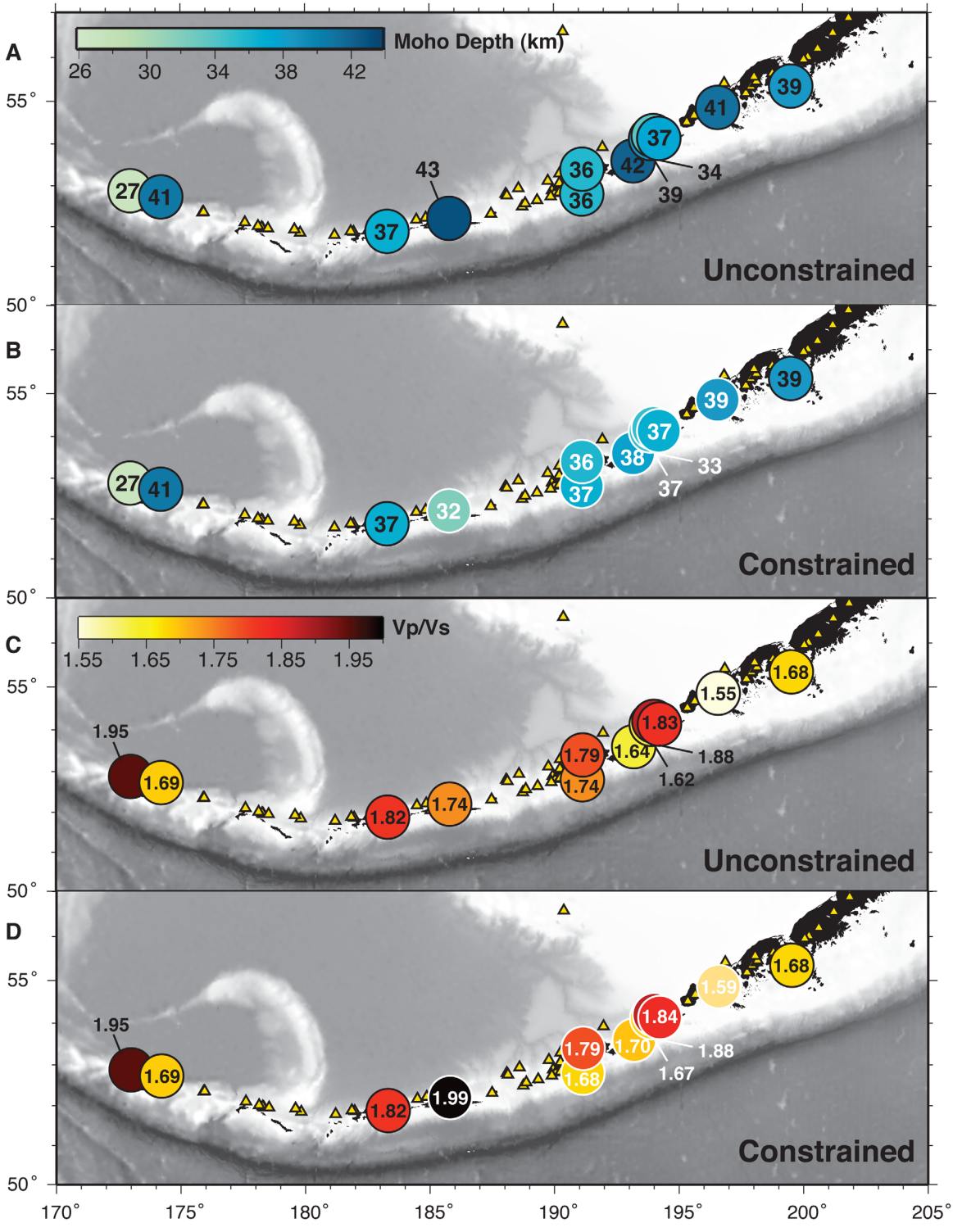

Figure 4. Summary of results (Table 2). Results from the single-layer inversion method are shown in black and those where interface depth is constrained by the active-source data are shown in white. (a) Moho depth results using the single-layer inversion method. (b) Moho depths including constraints from *Shillington et al.* [2004]. (c) Average crustal Vp/Vs results using the single-layer inversion method. (d) Average crustal Vp/Vs using the active-source Moho depth, where indicated.

not explained by simple models containing only the Moho boundary. These features must be due to complexities in the shallow crustal structure. Including a thin (<1 km thick) low-velocity near-surface layer (e.g., weathered layers, erupted lavas) can account for the discrepancy at many of the stations (section 3.3). Stations AKGG, AKUT, and AKRB on Akutan Island require more complex shallow crustal structures to explain early features (section 5.2).

3.2.3. Subducting Slab

[21] Several stations display evidence of the subducting crust. The Aleutian slab dips ~45°–55° and is ~65–95 km deep below the volcanic front [*Syracuse and Abers*, 2006], indicating that a slab Ps arrival can be expected in the receiver functions at lags of 7–11 s, between the upper-plate Ps and Ppms arrivals. Some stations show back-azimuthally varying, high-amplitude, positive pulses in this time range (see supporting information). In some cases, these are as strong or stronger than the Ps Moho arrival, similar to other receiver function studies imaging the subducting crust [*Ferris et al*., 2003]. The highest amplitude Ps phases are expected in traces that traveled updip [*Cassidy*, 1992], corresponding to arrivals from earthquakes in a range of back azimuths from NE to NW. Arrivals with these characteristics are seen at six stations: ADK, ATKA, ATTU, ATTUB, SDPT, and UNV (Figure 2). These stations span the entire range of the arc indicating the feature is present throughout, including under the far western Aleutians beyond where intermediate depth seismicity is seen [*Syracuse and Abers*, 2006].

3.3. Forward Modeling

[22] After inverting for crustal thickness and Vp/Vs, a synthetic receiver function is generated at each station using this crustal structure, and compared to the stacked receiver function data (Figure 5). Full-waveform receiver functions are calculated for plane-layered structure with a propagator-matrix method [e.g., *Haskell*, 1962]. These synthetics provide a test of the stacking method, and highlight those features in the receiver function stack that remain unexplained.

[23] At most stations the models predict the timing, width, and amplitude of the Moho Ps accurately. At NIKO and, to a lesser extent, NIKH the predicted arrival has higher amplitude than observed, probably due to the low velocity contrast at the Moho. For multiples, amplitudes generally did not agree as well and in several cases

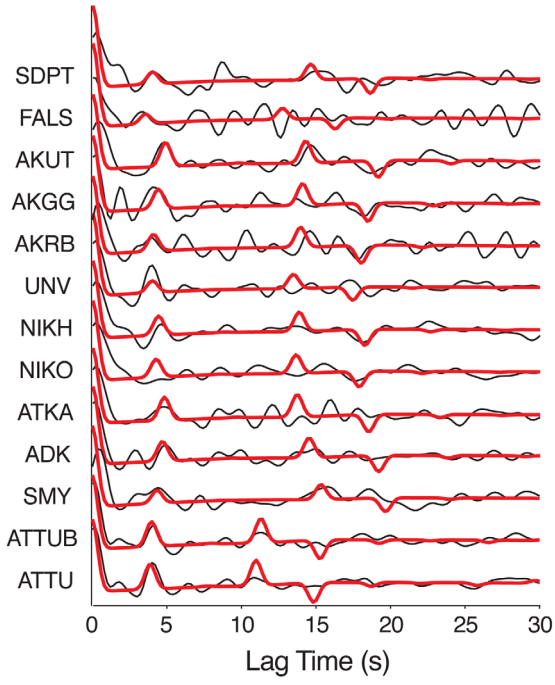

Figure 5. Comparison of receiver function stacks (black) and forward modeling results (red) using the Moho depth and Vp/Vs determined from the unconstrained inversion. These data, from Figure 2a, are for back-azimuths used to determine Moho depth in Figure 4. In some cases, secondary phases unrelated to Moho conversions are readily apparent.

the predicted Ppms and Psms amplitudes were larger than those observed. The receiver function inversions (e.g., Figure 3) assume that boundaries are abrupt and layer properties are constant, but real data are influenced by spatially varying and potentially gradational boundaries; hence, multiples predicted by the forward modeling are expected to have higher amplitudes than the data [*MacKenzie et al*., 2008]. Furthermore, the velocity contrast at the Moho might be lower than that predicted assuming a one-layer crust, if fast lower crust is present. In addition, ray parameter corrections are not applied in these stacks yet multiples display significant moveout over the range of ray parameters sampled, so stacking may reduce the multiples through destructive interference.

4. Discussion

4.1. Crustal Structure and Composition

[24] With the exception of crust beneath Attu island, receiver function results that are independent of active-source constraints indicate that the crust of the Aleutian island arc is 38.5 ± 2.9 km thick, where 2.9 km is the RMS variation of

individual measurements, and not much larger than the 2.6 km average uncertainty. Thus, crustal thickness remains relatively constant despite lateral changes in arc properties, including the westward transition from a continental to oceanic overriding plate, changes in obliquity and speed of convergence, increasing along-strike extension of the arc westward [*Freymueller et al.*, 2008], and changes in composition of primitive lavas or the parental arc magma [*Kelemen et al.*, 2003]. Our sampling of the arc is sparse and constrained to the locations of the islands, so there may be significant variability in crustal thickness at interstation wavelengths shorter than 50–100 km that would not be observed. Nonetheless, our data does reveal that there is comparatively little long-wavelength variation in crustal thickness along much of the arc. We would expect an increase in crustal thickness from the oceanic to continental sections due to thickness changes in preexisting crust, if magmatic productivity remained constant despite large changes in preexisting crustal thickness along the arc. Arc-normal convergence rate varies by $<10\%$ from ADK east to SDPT [*Syracuse and Abers*, 2006]. The observed consistency in crustal thickness implies that some process, either variation in magma production rate or differential erosion or foundering of the crust, must modulate crustal thickness along the arc. Age estimates for volcanic rocks in the Aleutians from $^{40}Ar/^{39}Ar$ dating show differences in ages of eruptive events along the arc [*Jicha et al.*, 2006] indicating that magma production may not be uniform. On the other hand, most island summits lie at elevations within 1000 m of sea level; thus, similar crustal thicknesses are balanced by similar elevations, perhaps indicating that erosion and isostasy act to keep crustal thickness roughly constant. We note that the small average velocity changes inferred from active-source data, roughly ± 0.2 km/s, correspond to average density changes of perhaps 100–200 kg/m^3, too small to significantly affect isostatic balance more than 1–2 km in crustal thickness.

[25] The average Vp/Vs of 1.77 indicates an intermediate to mafic crustal composition in the Aleutian island arc [*Zandt and Ammon*, 1995] and is higher than typical continental crust [*Christensen*, 1996; *Brocher*, 2005]. However, lower Vp/Vs appears to be present in the east than the west (Figure 6) more similar to that of continental crust [*Christensen and Mooney*, 1995; *Christensen*, 1996]. To first order, silica content is inversely proportional to Vp/Vs [*Zandt and Ammon*, 1995], at least in rocks with >55 wt % SiO_2 and bearing

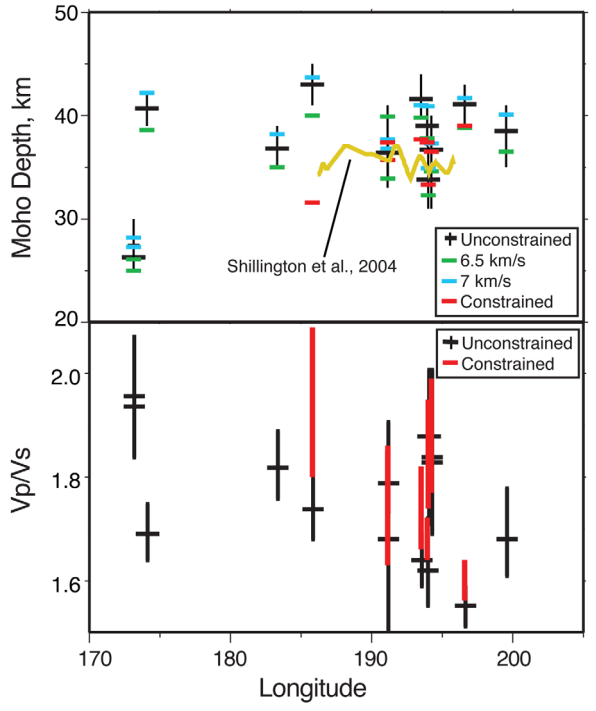

Figure 6. Moho depth and Vp/Vs versus station longitude along the arc. (top) Moho depth and error bars from the single-layer inversion method are shown in black. The Moho depth using Vp = 6.5 km/s is shown with green dashes, and the depth using Vp = 7 km/s is shown with blue dashes. The depth profile of the Moho predicted by *Shillington et al.* [2004] is plotted as a red line, and the red dashes indicate the Moho depth result when constrained to the active-source range. (bottom) The Vp/Vs estimates and error bars predicted by the single layer inversion are shown in black. The 85% confidence intervals for the active constrained results are shown as red rectangles.

quartz [*Hacker et al.*, 2003]. The change implies that the crust to the west is more mafic than that to the east. This variation in average crustal Vp/Vs corresponds with the change from continental to oceanic crust in the overriding plate, which should lead to a westward decrease in average silica content since the continental crust is expected to contain more evolved continental material.

[26] The other possible contribution to Vp/Vs is the composition of primary magmas, which can lead to changes in the crustal composition [*Kay and Kay*, 1994; *Kelemen et al.*, 2003]. Specifically, the concentration of MgO decreases and SiO_2 increases westward along the intraoceanic part of the arc [*Kay and Kay*, 1994; *Kelemen et al.*, 2003]. This should correspond to a westward decrease in Vp/Vs along the arc, to the extent that higher SiO_2 leads to lower Vp/Vs. This is the opposite of what we observe. Although Vp/Vs

increases with decreasing SiO_2 for many bulk compositions, rocks containing <55 wt % SiO_2 have minimal quartz and show a weak positive correlation between Vp/Vs and SiO_2 controlled by other phases [*Behn and Kelemen*, 2006]. For example, rocks with greater abundance of olivine and orthopyroxene tend to have lower Vp/Vs than rocks dominated by plagioclase or garnet [*Hacker et al*., 2003]. If most of the intruded lavas are sufficiently primitive that quartz is minor to absent, this trend would be expected. Primitive Aleutian arc magmas show SiO_2 ranging between 45 and 60 wt % in our study area and thus straddle both trends [*Kelemen et al*., 2003]. At least in the upper and middle crust, it is reasonable to expect more silicic compositions consistent with the lower observed Vp/Vs.

[27] In addition to the Moho boundary, a midcrustal boundary is observed at two stations in the central portion of the arc at ~20 km depth with a Vp/Vs of ~1.70 in the overlying section. The average Vp/Vs in the upper crust is lower than the total crustal Vp/Vs, suggesting that the Vp/Vs in the lower crust is higher. Such stratification is expected for many crustal differentiation scenarios that place more silicic rocks in the upper crust over a lower crust that is mafic. Additionally, elevated temperatures, presence of melt, and other factors that might be relevant to the lower crust beneath the active volcanic line would also serve to increase Vp/Vs in the deep part of the crust.

4.2. Previous Studies and Comparison to Other Arcs

[28] A small number of previous active-source seismic studies in the Aleutians provide a basis for comparison to this study. *Shillington et al*., [2004] present a *P* wave velocity model based on a sparse along-arc seismic refraction profile, 20–40 km south of the active volcanic line (but within the arc platform). The "unconstrained" Moho depths (those independent of the active-source data) are generally in agreement with the results from *Shillington et al*. [2004]—their study predicts an average crustal thickness from 35 to 37 km, while the average crustal thickness from this study is 38.5 km. This agreement is independent of our input *P* wave velocity assumption: even a very low crustal Vp of 6.5 km/s on average does not yield thicknesses less than 35 km (Figure 6). Our results more closely agree with the results of *Shillington et al*. [2004] and *Van Avendonk et al*. [2004] than the 30 km thick crust obtained by *Fliedner and Klemperer* [1999, 2000] in their analysis of the same profile, or equally thin crust (~30–32 km) seen on the cross lines [*Holbrook et al*., 1999; *Lizarralde et al*., 2002]. Six of the eight coincident stations have Moho error ranges that overlap with the depth range predicted by the *Shillington et al*. [2004] active-source data. The mid-crustal layer observed at approximately 20 km depth in *Shillington et al*., [2004] also is observed in this study intermittently.

[29] The Vp/Vs of the lower crust using active-source data by *Shillington et al*. [2013] yields somewhat lower values of Vp/Vs (1.7–1.75) than implied by our study. The active-source profile lies seaward of the active arc (and seaward of the arc crust sampled by receiver functions in this study). While crustal thickness is not expected to change considerably over the arc platform, there could be significant changes in temperature. Thus, lower Vp/Vs may be expected there owing to the absence of melt and lower temperatures [e.g., *Takei*, 2002]. Additionally, at lower temperatures, alpha quartz is stable at lower-crustal depths; even small (<5%) amounts can reduce Vp/Vs of the bulk composition substantially [*Ohno et al*., 2006; *Shillington et al*., 2013]. The Vp/Vs estimates from *Fliedner and Klemperer* [1999] agree with our results in the eastern section of the arc, but since their crustal thicknesses do not, it is not clear they can be compared.

[30] *Zandt and Ammon* [1995] characterize Poisson's ratio for different types of continental crust worldwide. While their sampling of island arcs is very limited and does not include the Aleutians, they suggest that the average arc has a Vp/Vs of 1.91 ± 0.16. This is higher than our measurements, but within their uncertainties. Studies elsewhere differ. The Izu-Bonin system exhibits substantial along-strike variations in average crustal thickness, from ~20 km in the Bonin arc to ~30 km in Izu [*Kodaira et al*., 2007a]; no published information on Vp/Vs exists for this area. This arc contains a thick region of relatively felsic material; it has been suggested that it may represent a more mature arc system than the Aleutians [*Tatsumi et al*., 2008]. In addition, large variations in crustal thickness (>10 km) are seen in the Izu-Bonin system on short (between volcanoes) scales [*Kodaira et al*., 2007a, 2007b], which are not seen here. These rapid variations in arc thickness have been interpreted to imply that focused crustal accretion and the generation of relatively felsic crust are occurring beneath large basaltic volcanoes in this arc. In Costa Rica, the crustal thickness ranges from 27.2 to 37.9 km while in Nicaragua it ranges

from 24.6 to 43.5 km including the forearc and backarc, and where differences in preexisting crust are known to exist [*MacKenzie et al.*, 2008]. Central America shows more crustal thickness variability than we observe in the Aleutians, which have comparable differences in preexisting crust. However, studies in the Aleutians do not have a sampling density comparable to these studies, and thus would miss volcano-spacing wavelength structure. But larger-scale variations are not observed.

5. Akutan Midcrustal Magma Body

5.1. Observations

[31] The stations on the island of Akutan—AKUT, AKGG, and AKRB—display a strong arrival in the first 3 s of their receiver functions (Figure 7a). The presence of this arrival varies with back azimuth and correlates with the location of the station relative to Akutan volcano (Figure 7b). This large positive arrival follows a sharp negative arrival in signals that have passed under the volcano at each of the stations. At AKGG, this signal is observed in most of the receiver functions (back-azimuth range ~90°–270°); its amplitude varies and is greatest between 150° and 270°. AKRB contains the signal in data from ~90° to 105° back azimuth. AKUT shows the signal in the ~220°–260° back-azimuthal range, although the negative pulse preceding it is not as large.

5.2. Magma Body Geometry

[32] To better delineate the magma chamber, we map the mode conversions it generates, by back-projecting signals along ray paths. The LVZ is considered present if a pulse arrives within 1–3 s after the initial *P* wave arrival and its amplitude is at least a quarter of the initial *P* wave (although many observed conversions have much larger amplitudes). The magma body appears to underlie much of the island, and extends farther east from the caldera than to the west of it (Figure 7). This feature is confined to the boundaries of the island at depth but is much larger in diameter than the edifice. Thus, we infer that the receiver functions show evidence for a large upper-crustal magma-rich body, based on the spatial distribution of signals, their high amplitude and back-azimuthal dependence.

5.3. Modeling

[33] Receiver functions from Akutan that showed evidence for the magma body are compared to

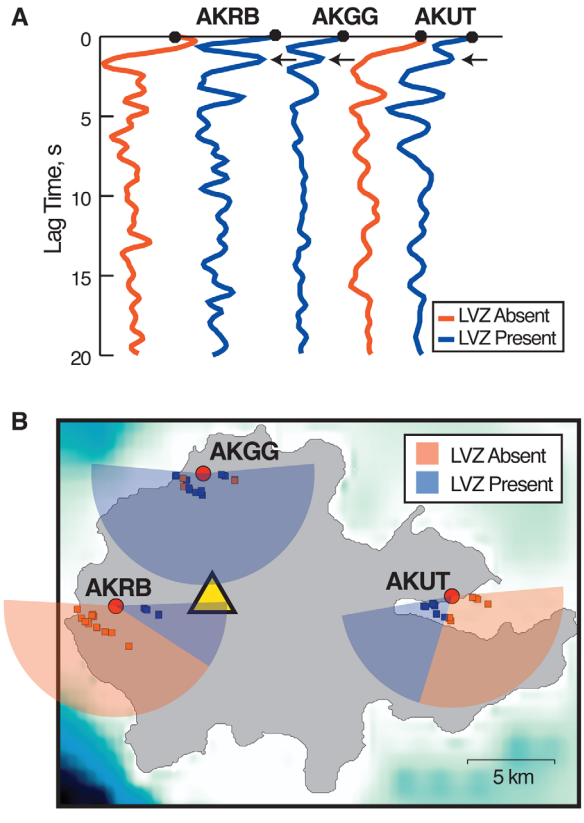

Figure 7. Back-azimuthal variation of the receiver functions from Akutan. (a) Stacks of the receiver functions for different back-azimuth ranges, corresponding to colors in Figure 7b. The black arrows denote the conversion from base of the LVZ. (b) Map of Akutan Island, showing stations (large circles), volcanic edifice (triangle), and the back-azimuthal ranges at which the LVZ conversions are observed (blue) or absent (orange). The squares show the piercing points of rays sampling the LVZ based on the modeled results, and the color indicates if the individual trace showed evidence of the layer (blue) or not (orange).

numerical models. At each station, four classes of models are generated (Figure 8); the exact velocities and depths varied slightly. Each has a boundary at <1 km depth to simulate a near-surface layer of cracked or porous rock. Model A additionally has a boundary at the Moho. Model B has a Moho boundary and a midcrustal boundary at approximately 20 km depth. Model C has the Moho and a shallow interface (~10 km depth). Model D has a ~2 km thick low-velocity layer near 10 km depth in addition to the Moho. These groups are compared to determine the underlying cause of the early signal. More precise depth and Vp/Vs estimates of those boundaries are determined by adjusting Vp/Vs and layer thickness to better match observed seismograms, via a simplex minimization [*Press et al.*, 1986] to match

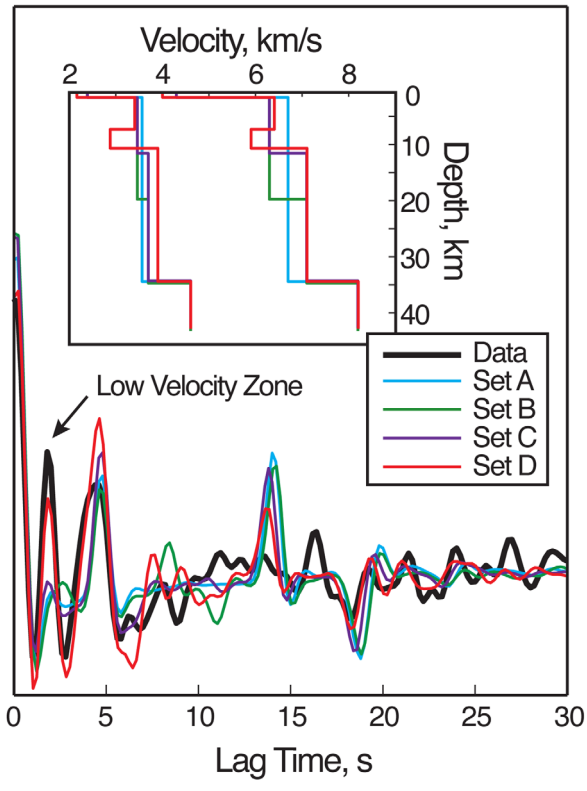

Figure 8. Four synthetic receiver functions generated to fit the data at AKGG compared with the actual data for that station, as described in text. Set D shown in red is the best fit model. Inset shows the corresponding velocity profiles.

observed to calculated receiver functions. This procedure kept the structure close to the initial model while matching data.

[34] Receiver functions that contain the early pulse are best fit by Model D at each station. Model D produces higher-amplitude pulses at 2–3 s, comparable to the Moho amplitude, and matches lag times better than the Models A-C. The model predicts some features after 7 s that do not appear in the data, perhaps due to attenuation or scattering of the later multiples, consistent with other receiver function studies of magma chambers [e.g., *Chmielowski et al*., 1999]. The final best fit models all contain a low-velocity surface-layer, a low-velocity layer representing the magma body around 9 km depth with high Vp/Vs, and the Moho boundary at a depth within the error range of that predicted by the single-layer inversion method (Figure 9).

[35] The low-velocity layer varies slightly in thickness and velocities at the three stations. The layer can be modeled assuming Vp = 5.9 km/s with a Vp/Vs of 2.05. The finite Vs implies that the layer is not liquid at seismic frequencies, and may be some sort of crystal-rich mush zone. It is located between approximately 7–10 km depth at AKGG, at 8.5–10.5 km depth at AKRB, and at 8–9 km depth at AKUT. The consistency of this feature across the three stations implies that it may be relatively continuous throughout the island, but thinner on the east of the island under AKUT, the station farthest from the caldera. Alternatively, there may be two magmatic centers on the western and eastern sides of the island that correspond to the clusters of seismicity observed in 1996 [*Lu et al*., 2000]. Additional modeling analysis may refine the precise velocities associated with this layer; however, the geometry and relative changes observed suggest that a body of partial melt is a robust explanation.

5.4. Interpretation and Comparison With Other Observations

[36] A few receiver functions studies on magma chambers exist. Consistent with our results, they report high-amplitude positive and negative features early in the receiver function, high Vp/Vs in the low-velocity zone (LVZ), spatial variation between receiver functions, and variations in the arrivals of multiples from deeper features (see supporting information for more details) [e.g., *Chmielowski et al*., 1999; *Wilson et al*., 2003; *Piana Agostinetti and Chiarabba*, 2008; *Abe et al*., 2010].

[37] Akutan volcano is one of the more active volcanoes within the Aleutians, with 31 eruptions since 1790 most recently in 1992, as well as subsequent seismicity, inflation, and steaming [*McGimsey et al*., 2011]. A seismic swarm in March 1996, inferred to have been at least in part caused by a magma intrusion, had epicenters between near-sea

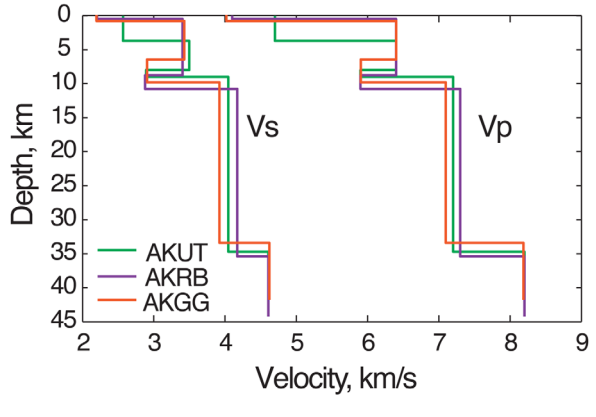

Figure 9. Velocity models describing the LVZ for each of the three stations on Akutan.

level to about 8 km in depth [*Lu et al.*, 2000]. This coincides with the estimated top of the magma body from the receiver function modeling results. Modeling of geodetic observations [*Lu et al.*, 2000] suggests that the top of a large Mogi-type magma source is located between 8 and 18 km. The receiver function LVZ is at the shallower end of the depth range; however, seismometers lie away from the volcanic summit. Furthermore, there is no reason to assume that inflation is restricted to a single low-velocity layer; Global Positioning System (GPS) measurements have been used to locate another magma source at approximately 3.9 km depth [*Ji and Herring*, 2011] indicating that magma storage under Akutan volcano is complex. These results indicate that receiver functions may be a useful, and thus far relatively unexplored, tool for analyzing magma systems.

6. Conclusions

[38] Receiver functions give the first arc-wide results of the Moho depth and crust-averaged Vp/Vs along the Aleutian island arc, and indicate that it is generally more mafic than continental crust. We observe a westward increase in Vp/Vs as the arc transitions from a continental arc to an oceanic arc, which we interpret to parallel a gradient in crust-averaged SiO_2 content. However, Moho depth remains constant at 38.5 ± 2.9 km despite these along-strike transitions in many arc parameters, perhaps because erosion and isostasy mediate crustal thickness. On the island of Akutan, three closely spaced seismic stations enabled us to image a low-velocity zone determined to be a large magma chamber or magma-rich body; with additional stations, features such as this may be observed on other islands. The complex receiver functions presented here demonstrate the need for a more densely spaced array of seismic stations to better resolve variations in Moho depth at the scale of volcano spacing, and to adequately sample other secondary features such as midcrustal boundaries, the subducting slab, and low-velocity zones.

Acknowledgments

[39] We like to thank the Lamont-Doherty Summer Intern Program, sponsored by the National Science Foundation REU Sites Program, for making this work possible. We also thank the IRIS DMC where the data are archived. This work was partially supported by the National Science Foundation award EAR-1015016 (Abers). We also gratefully acknowledge constructive reviews from Simon Klemperer and an anonymous reviewer, which greatly improved the manuscript.

References

Abe, Y., T. Ohkura, T. Shibutani, K. Hirahara, and M. Kato (2010), Crustal structure beneath Aso caldera, southwest Japan, as derived from receiver function analysis, *J. Volcanol. Geotherm. Res.*, *195*(1), 1–12, doi:10.1016/j.jvolgeores.2010.05.011.

Ammon, C. J. (1991), The isolation of receiver effects from teleseismic P-wave-forms, *Bull. Seismol. Soc. Am.*, *81*, 2504–2510.

Behn, M. D., and P. B. Kelemen (2003), Relationship between seismic P-wave velocity and the composition of anhydrous igneous and meta-igneous rocks, *Geochem. Geophys. Geosyst.*, *4*(5), 1041, doi:10.1029/2002GC000393.

Behn, M. D., and P. B. Kelemen (2006), Stability of arc lower crust: Insights from the Talkeetna arc section, south central Alaska, and the seismic structure of modern arcs, *J. Geophys. Res.*, *111*, B11207, doi:10.1029/2006JB004327.

Brocher, T. M. (2005), Empirical relations between elastic wavespeeds and density in the Earth's crust, *Bull. Seismol. Soc. Am.*, *95*(6), 2081–2092, doi:10.1785/0120050077.

Cassidy, J. F. (1992), Numerical experiments in broadband receiver function analysis, *Bull. Seismol. Soc. Am.*, *82*, 1453–1474.

Chmielowski, J., G. Zandt, and C. Haberland (1999), The central Andean Altopiano-Puna magma body, *Geophys. Res. Lett.*, *26*, 783–786.

Christensen, N. I. (1996), Poisson's ratio and crustal seismology, *J. Geophys. Res.*, *101*, 3139–3156.

Christensen, N. I., and W. D. Mooney (1995), Seismic velocity structure and composition of the continental crust: A global view, *J. Geophys. Res.*, *100*, 9761–9788.

DeMets, C., R. G. Gordon, D. F. Argus, and S. Stein (1994), Effect of recent revisions to the geomagnetic reversal time scale on estimates of current plate motions, *Geophys. Res. Lett.*, *21*, 2191–2194.

Ferris, A., G. Abers, D. Christensen, and E. Veenstra (2003), High resolution image of the subducted Pacific (?) plate beneath central Alaska, 50–150 km depth, *Earth Planet Sci. Lett.*, *214*, 575–588, doi:10.1016/S0012–821X(03)00403-5.

Fliedner, M. M., and S. L. Klemperer (1999), Structure of an island-arc: Wide-angle seismic studies in the eastern Aleutian Islands, Alaska, *J. Geophys. Res.*, *104*, 10,667–10,694.

Fliedner, M. M., and S. L. Klemperer (2000), Crustal structure transition from oceanic arc to continental arc, eastern Aleutian Islands and Alaska Peninsula, *Earth Planet Sci. Lett.*, *179*, 567–579.

Fournelle, J. H., B. D. Marsh, and J. D. Myers (1994), Age, character, and significance of Aleutian arc volcanism, in *Geology of North America, The Geology of Alaska*, vol. *G-1*, edited by G. Plafker and H. C. Berg, pp. 723–757, Geol. Soc. of Am., Boulder, Colo.

Freymueller, J. T., H. Woodard, S. Cohen, R. Cross, J. Elliott, C. Larsen, S. Hreinsdottir, and C. Zweck (2008), Active deformation processes in Alaska, based on 15 years of GPS measurements, in *Active Tectonics and Seismic Potential of*

Alaska, Geophys. Monogr. Ser., vol. *179*, edited by J.T. Freymueller et al., pp. 1–42, AGU, Washington, D. C.

Hacker, B. R., G. A. Abers, and S. M. Peacock (2003), Subduction factory: 1. Theoretical mineralogy, densities, seismic wave speeds, and H_2O contents, *J. Geophys. Res.*, *108*(B1), 2029, doi:10.1029/2001JB001127.

Haskell, N. A. (1962), Crustal reflection of plane P and SV waves, *J. Geophys. Res.*, *67*, 4751–4767.

Holbrook, W. S., D. Lizarralde, S. McGeary, N. Bangs, and J. Diebold (1999), Structure and composition of the Aleutian island arc and implication for continental crustal growth, *Geology*, *27*(1), 31–34.

Ji, K. H., and T. A. Herring (2011), Transient signal detection using GPS measurements: Transient inflation at Akutan volcano, Alaska, during early 2008, *Geophys. Res. Lett.*, *38*, L06307, doi:10.1029/2011GL046904.

Jicha, B. R., D. W. Scholl, B. S. Singer, G. M. Yogodzinski, and S. M. Kay (2006), Revised age of Aleutian island arc formation implies high rate of magma production, *Geology*, *34*, 661–664, doi:10.1130/G22433.1.

Jones, C. H., and R. A. Phinney (1998), Seismic structure of the lithosphere from teleseismic converted arrivals observed at small arrays in the southern Sierra Nevada and vicinity, California, *J. Geophys. Res.*, *103*, 10,065–10,090.

Jull, M., and P. B. Kelemen (2001), On the conditions for lower crustal convective instability, *J. Geophys. Res.*, *106*, 6423–6446.

Kay, R. W., and S. M. Kay (1988), Crustal recycling and the Aleutian arc, *Geochim. Cosmochim. Acta*, *52*, 1351–1359.

Kay, S. M., and R. W. Kay (1994), Aleutian magmas in space and time, in *Geology of North America, The Geology of Alaska*, vol. *G-1*, edited by G. Plafker and H. C. Berg, pp. 687–722, Geol. Soc. of Am., Boulder, Colo.

Kelemen, P. B., G. M. Yogodzinski, and D. W. Scholl (2003), *Along-strike variation in the Aleutian Island Arc: Genesis of high Mg# andesite and implications for continental crust, in Inside the Subduction Factory*, Geophys. Monogr. Ser., vol. *138*, edited by J. Eiler, pp. 223–276, AGU, Washington, D. C.

Kodaira, S., T. Sato, N. Takahashi, A. Ito, Y. Tamura, Y. Tatsumi, and Y. Kaneda (2007a), Seismological evidence for variable growth of crust along the Izu intraoceanic arc, *J. Geophys. Res.*, *112*, B05104, doi:10.1029/2006JB004593.

Kodaira, S., T. Sato, N. Takahashi, S. Miura, Y. Tamura, Y. Tatsumi, and Y. Kaneda (2007b), New seismological constraints on growth of continental crust in the Izu-Bonin intraoceanic arc, *Geology*, *35*, 1031–1034, doi:10.1130/G23901A.1.

Lizarralde, D., W. S. Holbrook, S. McGeary, N. Bangs, and J. Diebold (2002), Crustal construction of a volcanic arc, wide-angle seismic results from the western Alaska Peninsula, *J. Geophys. Res.*, *107*(B8), 2164, doi:10.1029/2001JB000230.

Lu, Z., C. Wicks, J. A. Power, and D. Dzurisin (2000), Ground deformation associated with the March 1996 earthquake swarm at Akutan volcano, Alaska, revealed by satellite radar interferometry, *J. Geophys. Res.*, *105*, 21,483–21,495.

MacKenzie, L., G. A. Abers, K. M. Fischer, E. M. Syracuse, J. M. Protti, V. Gonzalez, and W. Strauch (2008), Crustal structure along the southern Central American volcanic front, *Geochem. Geophys. Geosyst.*, *9*, Q08S09, doi:10.1029/2008GC001991.

McGimsey, R. G., C. A. Neal, J. P. Dixon, N. Malik, and M. Chibisova (2011), 2007 Volcanic activity in Alaska, Kamchatka, and the Kurile Islands: Summary of events and response of the Alaska Volcano Observatory, U.S. Geol. Surv. Sci. Invest. Rep. 2010–5242, 110 p.

Nikulin, A., V. Levin, and J. Park (2009), Receiver function study of the Cascadia megathrust: Evidence for localized serpentinization, *Geochem. Geophys. Geosyst.*, *10*, Q07004, doi:10.1029/2009GC002376.

Ohno, I., K. Harada, and C. Yoshitomi (2006), Temperature variation of elastic constants of quartz across the alpha-beta transition, *Phys. Chem. Miner.*, *33*, 1–9, doi:10.1007/s00269-005-0008-3.

Piana Agostinetti, N., and C. Chiarabba (2008), Seismic structure beneath Mt. Vesuvius from receiver function analysis and local earthquakes tomography: Evidences for location and geometry of the magma chamber, *Geophys. J. Int.*, *175*(3), 1298–1308, doi:10.1111/j.1365-246X.2008.03868.x.

Press, W. H., B. P. Flannery, S. A. Tekolsky, and W. T. Vetterling (1986), *Numerical Recipes: The Art of Scientific Computing*, 818 pp., Cambridge Univ. Press, New York.

Rossi, G., G. A. Abers, S. Rondenay, and D. H. Christensen (2006), Unusual mantle Poisson's ratio, subduction, and crustal structure in central Alaska, *J. Geophys, Res.*, *111*, B09311, doi:10.1029/2005JB003956.

Rudnick, R. L. (1995), Making continental crust, *Nature*, *378*, 571–578.

Rudnick, R. L., and D. M. Fountain (1995), Nature and composition of the continental crust: A lower crustal perspective, *Rev. Geophys.*, *33*, 267–309.

Sheehan, A. F., G. A. Abers, C. H. Jones, and A. L. Lerner-Lam (1995), Crustal thickness variations across the Colorado Rocky Mountains from teleseismic receiver functions, *J. Geophys. Res.*, *100*, 20,391–20,404.

Shillington, D. J., H. J. A. Van Avendonk, W. S. Holbrook, P. B. Kelemen, and M. J. Hornbach (2004), Composition and structure of the central Aleutian island arc from arc-parallel wide-angle seismic data, *Geochem. Geophys. Geosyst.*, *5*, Q10006, doi:10.1029/2004GC000715.

Shillington, D. J., H. J. A. Van Avendonk, M. D. Behn, P. B. Kelemen, and O. Jagoutz (2013), Constraints on the composition of the Aleutian arc lower crust from Vp/Vs, *Geophys. Res. Lett.*, *40*, 2579–2584, doi:10.1002/grl.50375.

Syracuse, E. M., and G. A. Abers (2006), Global compilation of variations in slab depth beneath arc volcanoes and implications, *Geochem. Geophys. Geosyst.*, *7*, Q05017, doi:10.1029/2005GC001045.

Takei, Y. (2002), Effect of pore geometry on VP/VS: From equilibrium geometry to crack, *J. Geophys. Res.*, *107*(B2), doi:10.1029/2001JB000522.

Tatsumi, Y., H. Shukuno, K. Tani, N. Takahashi, S. Kodaira, and T. Kogiso (2008), Structure and growth of the Izu-Bonin- Mariana arc crust: 2. Role of crust-mantle transformation and the transparent Moho in arc crust evolution, *J. Geophys. Res.*, *113*, B02203, doi:10.1029/2007JB005121.

Taylor, S. R. (1967), The origin and growth of continents, *Tectonophysics*, *4*(1), 17–34.

Van Avendonk, H. J. A., D. J. Shillington, W. S. Holbrook, and M. J. Hornbach (2004), Inferring crustal structure in the Aleutian island arc from a sparse wide-angle seismic data set, *Geochem. Geophys. Geosyst.*, *5*, Q08008, doi:10.1029/2003GC000664.

Wilson, C. K., C. H. Jones, and H. J. Gilbert (2003), Single-chamber silicic magma system inferred from shear wave discontinuities of the crust and uppermost mantle, Coso geothermal area, *California, J. Geophys. Res.*, *108*(B5), 2226, doi:10.1029/2002JB001798.

Yogodzinski, G. M., J. L. Rubenstone, S. M. Kay, and R. W. Kay (1993), Magmatic and tectonic development of the western Aleutians: An oceanic arc in a strike-slip setting, *J. Geophys. Res.*, *98*(B7), 11,807–11,834, doi:10.1029/93JB00714.

Zandt, G., and C. J. Ammon (1995), Continental crust composition constrained by measurements of crustal Poisson's ratio, *Nature*, *374*, 152–154.

Zandt, G., S. C. Myers, and T. C. Wallace (1995), Crust and mantle structure across the Basin and Range—Colorado Plateau boundary at 37°N latitude and implications for Cenozoic extensional mechanism, *J. Geophys. Res.*, *100*, 10,529–10,548.

Zhu, L., and H. Kanamori (2000), Moho depth variation in southern California from teleseismic receiver functions, *J. Geophys. Res.*, *105*, 2969–2980.